CIMAC CONGRESS 25
ZURICH, MAY 19 – 23, 2025

2025 | 205

Partial cracking ammonia for marine engine applications: from mechanism to numerical investigation

Basic research & advanced engineering - new concepts

Yuan Fang, Dalian university of technology

Wenjing Qu, Dalian university of Technology
Liyan Feng, Dalian university of Technology

ABSTRACT

The utilization of ammonia in internal combustion engines faces challenges due to its inherently inert combustion characteristics and potential nitrogen emissions. The trend of blending ammonia with diesel or hydrogen for combustion in engines is unfolding. For large-bore marine engines, the strategy of using diesel to ignite ammonia can significantly improve the ignition characteristics of the mixture without requiring a high compression ratio. However, due to the large bore size of marine engines, the combustion of premixed ammonia/air mixtures that are not directly ignited by diesel is often limited by the inherently slow combustion rate of ammonia. The addition of hydrogen can address the issue of slow flame speed in the premixed gases, thereby increasing the degree of constant-volume combustion and enhancing the engine's performance. Ammonia can produce hydrogen in situ through heat-assisted catalytic reforming, using exhaust gases as heat sources. This approach allows hydrogen production for fueling marine engines without the need for expensive onboard hydrogen storage and transportation equipment.

In this study, we experimentally obtained the ignition delay times (IDTs) of NH3/H2/N2/n-heptane mixtures under high-pressure conditions using a rapid compression machine (RCM). In this context, N2 and H2 are derived from the decomposition of NH3, and n-heptane serves as a diesel surrogate. Based on these ternary fuel mixture experiments and extensive data collection on NH3/H2 and NH3/n-heptane combustion, we developed a reduced chemical mechanism for the ternary fuels using an evolution algorithm. This new reduced mechanism was extensively validated against various experimental data in the literature, including IDTs and laminar burning velocities (LBVs), making it suitable for predicting the combustion of ternary fuels in engines. Subsequently, we conducted numerical studies on a low-speed two-stroke marine engine with a bore diameter of 340mm, focusing on diesel-ignited partially cracked ammonia mixtures. We examined the effects of NH3 cracking ratios and excess air coefficients on engine performance and emissions, including unburned ammonia. Our systematic analysis of different ammonia decomposition levels revealed an operating window, where adjustments to the excess air coefficient were made to balance various trade-offs. Comparing scenarios with and without ammonia decomposition, it was shown that engines using partially cracked ammonia achieved significant performance improvements and reduced unburned ammonia emissions.

This research begins with mechanism development, employing a rigorously validated reduced mechanism to conduct CFD studies. It provides an in-depth exploration of the ammonia partial cracking strategy, aimed at enhancing ammonia utilization as a zero-carbon fuel in marine engine applications. This work advances the understanding of performance and emissions for large-bore ammonia-fueled engines.

1 INTRODUCTION

Ammonia (NH_3) is widely accepted as one of the promising zero-carbon fuels to be used in internal combustion engines (ICE) to reduce carbon emissions. The production, storage, and transportation infrastructure for ammonia is well-established thanks to mature agricultural systems [1, 2]. However, in terms of its utilization in compression ignition and spark ignition ICEs, pure ammonia has high resistance to combustion, specifically, a high latent heat of vaporization, a narrow flammability range, high ignition resistance, low combustion temperature, and low burning rate [3]. In recent years, in the field of internal combustion engines, the stable combustion and emission control of ammonia as a fuel have received growing interest [4-6].

To enhance the combustion of ammonia, strategies of adding other high reactivity fuels, such as diesel, dimethyl ether (DME), hydrogen (H_2), and methane, to achieve high-quality combustion have been an unfolding trend. Specifically, blending ammonia with high cetane number fuels like diesel can significantly improve the ignition characteristics of the mixture [7]. For pure ammonia, extremely high compression ratios from 35:1 to 100:1 are needed to achieve stable compression ignition operation [8], which is unpractical in ICEs. However, with the addition of diesel, stable compression ignition can be achieved at a lower compression ratio. Currently, ammonia/diesel dual-fuel engines only require simple modifications to the existing engines, enabling an immediate short-term reduction in carbon emissions. This has led to increasing research on ammonia/diesel co-combustion [9-11]. Recently, engines utilizing ammonia and hydrogen have been widely studied, primarily focusing on spark ignition methods [12]. When hydrogen is added to ammonia, the presence of H_2 increases the formation of O, H, and OH radicals [13] thereby facilitating the oxidation process. Adding H_2 not only enhances the autoignition characteristics of NH_3 to a certain extent [14], but more significantly, the co-combustion of these two gaseous fuels efficiently accelerates the flame propagation and broadens the flammability limits compared to pure NH_3 [15].

Hydrogen, as another commonly used carbon-free clean fuel, has been extensively studied for its blend combustion with ammonia due to its inherent flammability [16]. The combustion mechanism of NH_3/H_2 mixtures has recently received widespread attention in the combustion research field. Mei et al. [15] found that at an equivalence ratio of 1.1 and a pressure of 1 atm, the laminar burning velocities (LBVs) of a mixture with 40% cracked NH_3 and air reached 38.1 cm/s, comparable to the LBVs of a methane/air mixture under the same conditions. Recently, Klawitter et al. [17] found that under high-pressure engine conditions, a 10% NH_3 cracking ratio is sufficient to achieve flame speeds comparable to CH_4 in lean fuel/air mixtures with highly turbulent flow conditions.

Due to the inherent safety risks associated with hydrogen storage and utilization, ammonia, as an energy carrier containing 17.6 wt% hydrogen, can be thermally decomposed to produce hydrogen [18]. This process addresses the challenges of hydrogen storage, transportation, and safety issues [19] , which limit the practical applications of hydrogen as a standalone fuel [20]. Hydrogen production from onboard ammonia decomposition is applicable for fueling marine engines [21]. Unlike the complete conversion required for ammonia decomposition to supply hydrogen for fuel cells, partial decomposition of ammonia for engine applications does not require high hydrogen purity [22, 23]. The partial decomposition of ammonia for engine applications has been explored in various studies [24-28]. Frigo et al. [24] confirmed the necessity of ammonia-hydrogen co-combustion by blending hydrogen obtained from ammonia through onboard catalytic reforming. Lhuillier et al. [25] and Ryu et al. [26] experimentally used hydrogen generated in situ through NH_3 catalytic or heat-assisted dissociation as a combustion promoter, achieving enhanced performance. Comotti et al. [27] employed a hydrogen generation system that uses exhaust gases as heat sources to crack ammonia in situ. Ezzat et al. [28] demonstrated that producing hydrogen onboard via the electrochemical splitting of ammonia in an electrolyte cell was sufficient to fuel the internal combustion engine. Gill et al. [29] simulated the partial decomposition of ammonia by using bottled gases of ammonia, nitrogen, and hydrogen. They investigated the combustion and emissions characteristics of using H_2, NH_3, and dissociated NH_3 as a dual-fueling approach with diesel fuel.

In engine numerical simulations, n-heptane is commonly used as the substitution of pilot diesel. Moreover, the premixed combustion phase relies heavily on the combustion characteristics of the NH_3/H_2 mixture, with a particular emphasis on flame propagation. This aspect is critical for accurately reflecting the heat release rate, cylinder pressure changes, and overall engine performance. Consequently, studying the reduced mechanism of partially cracked ammonia and n-heptane mixtures is essential for precise simulation under these conditions.

For systems involving ammonia, mechanisms developed for pure NH_3 are often not suitable for NH_3/H_2 mixtures. The current NH_3 combustion mechanisms are still inadequate at accurately

predicting the flame characteristics of NH_3/H_2 combustion [30]. Due to the later development of nitrogen-containing mechanisms specific to ammonia, new effective reaction pathways and updated reaction rates continue to emerge. Currently, there are numerous NH_3/H_2 blending mechanisms that exhibit varied performance in describing combustion characteristics such as ignition delay times (IDTs), LBVs, among others. Rocha et al. [31] evaluated ten mechanisms for predicting laminar flame speeds, and the results were scattered. Noted that, due to the varying conditions under which different models were developed, their direct applicability to other NH_3/H_2 blends is limited. Developed from the pure ammonia mechanism by Shrestha et al. [32], the NH_3 mechanism by Mei et al. has undergone multiple updates by their team to extend its applicability from NH_3/H_2 to mixtures involving partially cracked ammonia [15, 33, 34]. Han et al. [35] also observed that many mechanisms do not perform well in predicting pre-dissociated NH_3/air flames under the conditions they studied, even for those mechanisms that accurately predict NH_3/H_2/air flames. On the other hand, according to our previous research, mechanisms developed for pure n-heptane also show reduced accuracy when predicting combustion under hydrogen-rich conditions [36].

To conclude, using n-heptane to ignite mixtures of partially decomposed NH_3 (producing $NH_3/H_2/N_2$) is a feasible approach to enhance ammonia engine performance. In terms of the mechanism, previous investigations have extensively focused on blending mechanisms for NH_3/H_2 and NH_3/n-heptane binary fuels. However, it is not feasible to use NH_3/n-heptane binary blending mechanisms to study ternary fuels containing H_2 or under partially cracked ammonia conditions. Therefore, it is essential to study the ternary mechanism of NH_3/H_2/n-heptane after hydrogen addition, as a high-fidelity mechanism is crucial for accurate numerical simulations. Regarding numerical simulations, although many researchers have investigated the use of partially cracked ammonia as a fuel in spark-ignition (SI) engines, to the best of the authors' knowledge, there is currently no research exploring the operating window of ammonia cracking ratios and excess air coefficients in numerical simulations of mixtures with partially cracked ammonia ignited by diesel in compression-ignition (CI) engines.

The present study investigates the compression ignition characteristics of NH_3/H_2/n-heptane ternary fuels at various blending ratios. Additionally, a novel method for developing reduced mechanisms for these ternary fuels was introduced. This reduced mechanism was further optimized using an evolutionary algorithm (EA) to ensure its accuracy in predicting the combustion behavior of ternary fuels under engine-relevant conditions. The new reduced mechanism underwent extensive validation against a wide range of experimental data available in the literature, including IDTs and LBVs. Finally, the mechanism was applied to systematic engine condition simulations to explore the effects of varying NH_3 cracking ratios and excess air coefficients (λ).

2 METHODOLOGY

2.1 EXPERIMENTAL METHODS

2.1.1 RAPID COMPRESSION MACHINE FACILITY

The compression ignition characteristic experiments were conducted using a rapid compression machine (RCM) from Dalian University of Technology. Figure 1 shows the schematic diagram of the RCM structure.

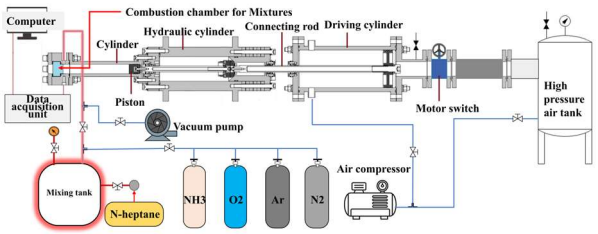

Figure 1. Schematic diagram of the heated RCM.

The details of this experimental setup have been previously described in the literature [37, 38]. Briefly, the mixing tank, combustion chamber, and cylinder head of the RCM were heated to maintain a controlled experimental temperature. Cylinder pressure was measured using a pressure sensor (AVL GH14DK), and the temperature was calculated based on the "adiabatic core" hypothesis [39] using the following formula:

$$\int_{T_0}^{T_C} \frac{\kappa(T)}{\kappa(T)-1}\frac{dT}{T} = ln\left(\frac{P_C}{P_0}\right) \quad (1)$$

Where $\kappa(T)$ refers to the specific heat ratio of the specific mixture as a function of temperature.

In practical operation, the compression process and the thermodynamic behavior at top dead center (TDC) were not ideal adiabatic due to heat loss from heat conduction and gas leakage from the piston rings. To account for these facility-related effects, non-reactive measurements were also conducted by replacing O_2 with N_2 for every experimental mixture. All pressure/time data were subsequently converted into volume/time profiles for subsequent use in the chemical simulations. The definition of IDTs is the time interval between

the end of compression (EOC) and the moment of maximum pressure rise rate (d*p*/dt), which represents the ignition timing. Meanwhile, corresponding non-reactive pressure trace was also presented for comparison.

The measurement uncertainties in the RCM experiments are influenced by several factors, with the calculated compressed temperature (Tc) being a primary contributor. Following the uncertainty calculation method outlined by He et al. [40], the uncertainty of the experimental data in the present study is estimated to be within 20%.

2.1.2 EXPERIMENTAL MIXTURES PREPARATION

Gas mixtures were pre-mixed in the mixing tank, and the temperature was controlled to ensure that the partial pressure of n-heptane did not exceed half of its saturated vapor pressure. During both gas preparation and the introduction of NH_3-containing mixtures into the RCM, the passivation method described by Mathieu et al. [41] was applied to ensure the ammonia adsorption-desorption equilibrium on the surface of stainless steel equipment, thereby reducing the proportional error of ammonia in the mixture. The quoted purities of argon, oxygen, ammonia, and nitrogen used in the present experiments all exceeded 99.99%, while liquid n-heptane had a purity level exceeding 99.5%. Table 1 summarizes the molar composition of all mixtures in the current experiments, with air serving as the oxidizer for all cases. The fuel introduced into the mixing tank was categorized into liquid and gaseous fuels. The Gaseous fuel ratio in Table 1 represents the molar proportion of NH_3 and H_2, while the n-heptane fraction indicates the proportion of n-heptane in the total fuel, which can be expressed using the following formula:

$$X_{n-heptane} = \frac{n_{n-heptane}}{n_{n-heptane}+n_{NH_3}+n_{H_2}} \quad (2)$$

where n represents the molar quantity of each substance in the mixing tank.

In the present work, the effect of the ammonia cracking ratio on IDT was studied based on Mixture 1, which represents the initial state with a 0% ammonia cracking ratio. Subsequently, the partial cracking ratio was progressively increased by decomposing ammonia in the mixture until it reached 100%. This mathematical definition of γ, consistent with that proposed by Mei et al. [15], defines the NH_3 partial cracking ratio as the proportion of cracked ammonia moles to the initial ammonia moles. It can be expressed as:

$$\gamma = \frac{n_{NH_3\_cracked}}{n_{NH_3\_init}} \quad (3)$$

where $n_{NH_3\_cracked}$ and $n_{NH_3\_init}$ represent the concentrations of cracked and initial ammonia, respectively, and n indicates the corresponding molar amount.

In summary, the experiments were conducted across a wide range of fuel compositions and thermal operating conditions. The NH_3/H_2 ratio varied from 0% to 100%, while n-heptane was tested at proportions of 5%. The Tc ranged from 650 K to 1050 K, and the compressed pressure (Pc) ranged from 15 to 30 bar. Notably, for partially cracked ammonia, the cracking ratio was systematically varied from 0% to 100% to comprehensively investigate its effect on IDTs.

Table 1. Mixture compositions (in molecular terms)

Mixtures	Oxidizer	Molar ratio of gaseous fuels		Liquid fuel fraction (of total fuels)	ϕ	NH_3 partial cracking ratio
		xNH_3	xH_2	$X_{n\text{-heptane}}$		γ
1	air	100%	0%	0.05	1	0
2	air	90%	10%	0.05	1	0
3	air	70%	30%	0.05	1	0
4	air	40%	60%	0.05	1	0
5	air	0%	100%	0.05	1	0
6	air	70%	30%	0.05	0.5	0
7	air	70%	30%	0.05	2	0
8	air	100%	0%	0.05	1	30%
9	air	100%	0%	0.05	1	10%
10	air	100%	0%	0.05	1	100%

2.2 KINETIC SIMULATION METHODS

All chemical kinetics simulations in this study were performed using an in-house Cantera-based program. The IDTs for shock tube were simulated using a zero-dimensional adiabatic reactor model with a constrained volume, assuming ideal conditions for solving the energy equation. For IDT simulations in the RCM, a homogeneous reactor model was employed, incorporating a case-specific volume profile for each scenario.

The LBVs were simulated using a one-dimensional, freely propagating laminar premixed flame model combined with a mixture-averaged transport model. A relatively dense computational grid was applied with slope and curvature criteria set to 0.02 and 0.04, respectively, and the maximum number of grids allowed was 2000. Thermal diffusion was neglected in these simulations.

The IDT for the shock tube was defined as the time interval between the start of the simulation and the point of maximum slope in the OH concentration profile. The definition of IDT for the RCM has been provided earlier in the text.

2.3 NUMERICAL ENGINE MODELING AND SIMULATION METHODS

In the present study, a three-dimensional CFD simulation of a low-speed, two-stroke marine partial-cracking ammonia/diesel (PCAD) engine was conducted using CONVERGE 3.0. The engine under investigation was a modified version of a prototype diesel engine. The basic specifications and timing parameters of the modified PCAD engine are listed in the Table 2. A pre-chamber was added to enhance the combustion of the pre-mixture, as depicted in Figure 2. Detailed information about the pre-chamber design, computational models, adaptive mesh refinement strategy, grid sensitivity analysis, and validation of pure-diesel mode simulations against experimental data can be found in our previous works [42].

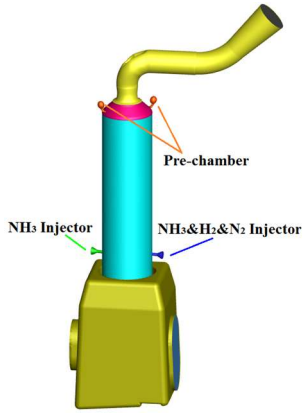

Figure 2. Schematic diagram of the PCAD engine model.

For this study, the primary modifications included the redesign of the gas fuel injection system. Referring to designs of low-speed, two-stroke marine natural gas and hydrogen engines [38], two low-pressure gas injectors were installed on the midsection of the cylinder liner, as shown in Figure 2. One injector was designated for ammonia injection, while the other was used to inject partially cracked ammonia—a blended gas mixture of ammonia, hydrogen, and nitrogen, with a hydrogen-to-nitrogen ratio of 3:1 based on the atomic ratios of hydrogen and nitrogen in ammonia. It is noteworthy that the actual cracking ratio of ammonia for this blending gas injector differs from the nominal cracking ratio γ. The actual cracking ratio refers to the fraction of ammonia that has undergone decomposition during the cracking operation, excluding the ammonia injected by the dedicated ammonia-only injector. In contrast, γ represents the nominal cracking ratio, which accounts for all injected gas fuel. The calculation of γ includes the contribution of ammonia injected through the ammonia-only nozzle. By adjusting the gas blending ratio in the $NH_3/H_2/N_2$ injector, different partial cracking ratios of ammonia can be achieved.

Table 2. Engine model specification.

Type	Parameter
Bore /mm	340
Stroke /mm	1600
Compression ratio (CR)	19.8
Rotate speed /rpm	157
Exhaust valve open /°CA	110-275
Calculation interval/°CA	110-470
Scavenging interval/°CA	140-220
Gas fuel injection timing /°CA	245
Diesel injection timing /°CA	360

With the presence of hydrogen, the combustion velocity increases significantly, which can lead to excessive in-cylinder peak pressures. To mitigate this issue, it is common to reduce either the compression ratio or the total energy input. In this study, the compression ratio remains unchanged from the prototype diesel engine (19.8). Instead, adjustments were made to the total energy input.

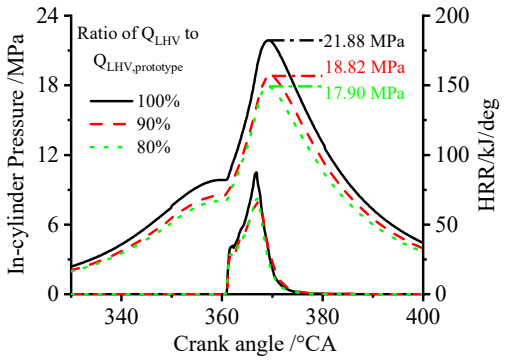

Figure 3. Comparison of in-cylinder pressure and HRR under different Q_{LHV} conditions for a PCAD engine. The energy ratio of ammonia to hydrogen is set at 90:10, with diesel ignition energy contributing 2.5% of the total fuel energy.

Figure 3 illustrates the comparison of in-cylinder pressure and heat release rate (HRR) under different Q_{LHV} conditions, where Q_{LHV} refers to the total energy introduced to the cylinder based on the lower heating value. From Figure 3, it can be concluded that when the total fuel calorific value is equivalent to that of the prototype diesel engine, the maximum in-cylinder pressure reaches 21.88 MPa—nearly 20% higher than the prototype diesel engine. However, when the total fuel calorific value

is reduced to 80% of the prototype diesel engine's calorific value, the maximum in-cylinder pressure is 17.9 MPa, meeting safety requirements. Therefore, the total fuel calorific value is set to 80% of that of the prototype diesel engine.

3 COMBUSTION REACTION MECHANISM DEVELOPMENT

The detailed and complex chemical reaction mechanisms are not suitable for engineering applications due to their computational demands; therefore, reduced mechanisms are typically employed. However, reduced mechanisms cannot fully preserve the predictive capability of the detailed mechanism across all operating conditions, especially when there is a need to minimize the mechanism size to reduce CFD computational resources and development time. This paper introduces a new approach for mechanism reduction, termed the Scenario-Decoupled Mechanism Reduction Method (SDMRM). The core idea of this method is to break down the combustion process into specific chemical research targets and the dominant chemical reactions governing combustion for a given scenario. The approach retains reaction pathways and reactions that exhibit strong correlations, while removing those with minimal impact or that are not dominant. Despite this, the retained reaction pathways are still reduced. To compensate for the potential distortion in simulation predictions caused by the reduction of the mechanism, we utilize a multi-objective EA to optimize the sensitivity coefficients of the key reactions for the relevant operating conditions. In particular, for the PCAD engine, where diesel serves as an ignition fuel, the scenario-decoupling mechanism reduction process is illustrated in Figure 4. It highlights the chemical process of the PCAD engine and its corresponding chemical research objectives, along with the scope of mechanism validation data.

In present work, the initial mechanism for ammonia/n-heptane combustion was developed based on the binary-fuel mechanism proposed by Alekseev et al. [43] which includes only 157 reactions. This mechanism, originally derived from the detailed NH_3/n-heptane mechanism by Thorsen et al. [44] underwent extreme reduction to make it specifically designed for combustion prediction under engine operating conditions. For our scenario-based mechanism reduction strategy, such a well-reduced ammonia/n-heptane mechanism is desirable.

The C0 reactions related to ammonia, specifically the NH_3/H_2 sub-mechanism, are directly linked to the combustion and emission characteristics of PCAD engines. To address the deficiencies in the NH_3/H_2 sub-mechanism within the initial NH_3/n-heptane mechanism, we utilize the NUIG2023 detailed mechanism [45], which has been comprehensively validated against available data from fundamental combustion experiments to describe the combustion of NH_3/H_2 mixtures. This replaces the zero-carbon reactions in the underlying mechanism. Research by Girhe et al. [46] demonstrates that by quantifying the agreement between experimental data and their computed counterparts across a wide range of combustion data categories for various kinetic models, the NUIG2023 model provides the best performance in predicting NH_3/H_2 systems in terms of overall accuracy, particularly excelling in high-temperature oxidation speciation.

During the development of the ternary mechanism, improvements to the C0 mechanism of NH_3/H_2 inevitably result in changes to the performance of the NH_3/n-heptane mechanism, in accordance with the decoupling principle. Therefore, after incorporating sub-mechanisms that perform well in predicting LBV and NH_3/H_2 combustion characteristics, it is necessary to re-optimize and validate the NH_3/n-heptane sub-mechanism to ensure it accurately reflects the auto-ignition characteristics of NH_3/H_2/n-heptane mixtures. We employed an EA to optimize the mechanism, and the optimization process is illustrated in Figure 5.

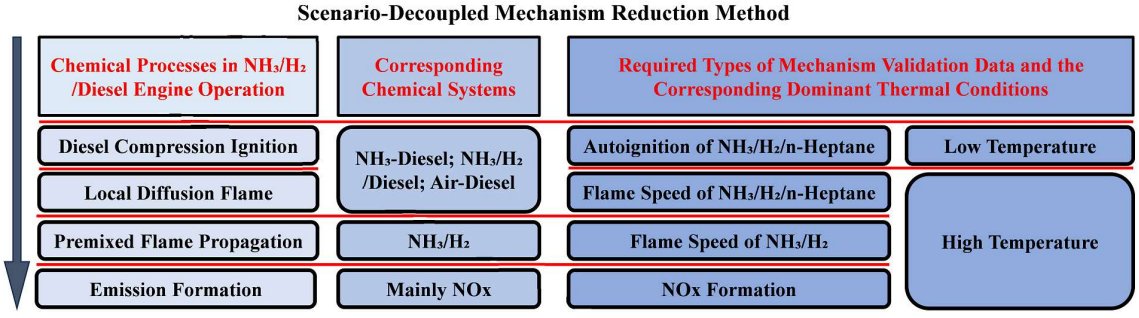

Figure 4. Analysis process of PCAD engine based on the scenario-decoupled mechanism reduction method.

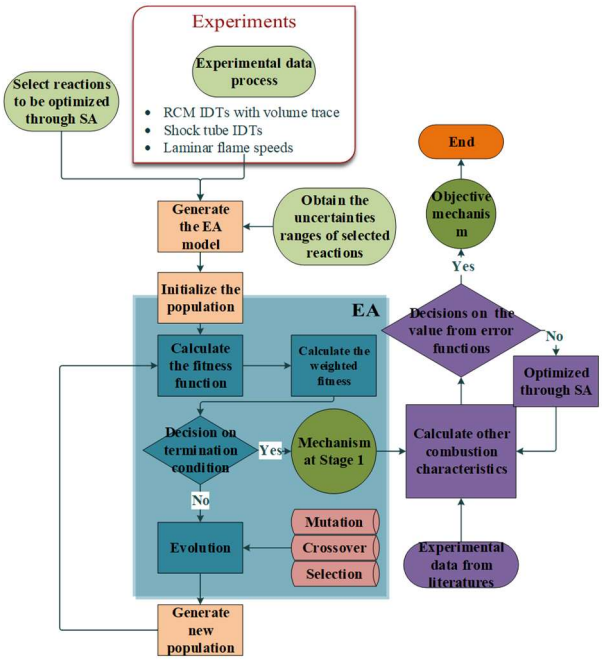

Figure 5. Diagram of the model optimization process based on the evolutionary algorithm

The EA has been demonstrated to be highly suitable for optimizing chemical mechanisms in high-dimensional parameter spaces [47]. Before initiating the optimization process, a population of multiple individuals is generated. Each individual comprises a set of genes, with the number of genes corresponding to the elementary reactions whose pre-exponential factors require optimization. The range of each gene is defined as the permissible range of the multiplicative factor associated with the pre-exponential factor. During the crossover and mutation phases of the genetic process, the gene values are manipulated in the logarithmic space, ensuring that the multiplicative factor is transformed into a linear operation.

The optimization process is guided by a primary fitness function, which consists of two key sub-functions: the IDT fitness and the LBV fitness. Both sub-functions are expressed as the average relative error between experimental and simulated results. However, since flame speed errors are typically smaller than IDT errors, a weighting factor is applied to the fitness calculation for specific target conditions to enhance optimization efficiency. The fitness function formulas are expressed as follows：

$$F_{IDT} = \frac{1}{N}\sum_{i=1}^{N} w_i \left|\frac{IDT_{sim,i} - IDT_{exp,i}}{IDT_{exp,i}}\right| \quad (4)$$

$$F_{LBV} = \frac{1}{M}\sum_{j=1}^{M} w_j \left|\frac{LBV_{sim,j} - LBV_{exp,j}}{LBV_{exp,j}}\right| \quad (5)$$

$$F_{total} = \alpha F_{IDT} + \beta F_{LBV} \quad (6)$$

where N and M represent the number of target conditions, wi and wj are the weighting factors for the corresponding conditions, and α and β are the weighting factors for IDT and LBV fitness, respectively.

4 RESULT AND DISCUSSION

4.1 MEASURED AND SIMULATED CHEMICAL RESULT

4.1.1 VALIDATION OF IDTS

The high-pressure IDTs under varying ammonia-hydrogen ratios, equivalence ratios, and ammonia cracking rates were experimentally measured at compressed pressures of 30 bar and 15 bar using an RCM apparatus. Figure 6-8 compare the experimental data with predictions from the reduced mechanism optimized through the evolutionary algorithm. In these figures, the lines represent the predictions of the present reduced mechanism, while the points denote the experimentally measured data. Overall, the simulation results of the current model show close agreement with the experimental data.

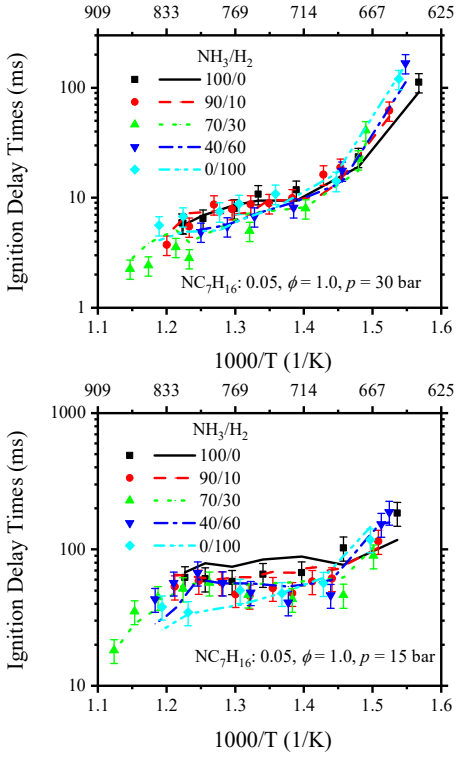

Figure 6. Measured (points) and calculated (lines) IDTs for NH_3/H_2/n-heptane mixtures with different NH_3/H_2 ratios, at ϕ = 1, and Pc of 30 bar and 15 bar.

Figure 6 presents the comparison of IDTs as a function of the inverse temperature under fixed conditions where n-heptane accounts for 5% of the total fuel molar ratio. The blending ratios of hydrogen and ammonia in the gaseous fuel vary

from pure ammonia to pure hydrogen (in molar ratios). The results indicate that the IDTs for most mixtures are close under the same thermodynamic conditions, suggesting that the apparent ignition characteristics of ternary fuel mixtures with varying NH_3/H_2 ratios are similar under these conditions. The reactivity of the NH_3/H_2/n-heptane mixtures remains predominantly governed by the intrinsic reactivity of n-heptane. As depicted, IDTs generally decrease with increasing temperature and pressure across all mixtures. However, due to the presence of n-heptane, a negative temperature coefficient (NTC) behavior is observed at Pc = 15 bar in the temperature range of 730 K to 800 K. Despite the overall similarity, subtle differences in IDTs can still be discerned with varying NH_3/H_2 ratios. At lower temperatures, mixtures with higher ammonia content generally exhibit shorter IDTs. As the temperature rises, the IDTs of hydrogen-rich mixtures decrease more rapidly. At around 690 K, a crossover in the IDT curves is observed for several mixtures at both 15 bar and 30 bar.

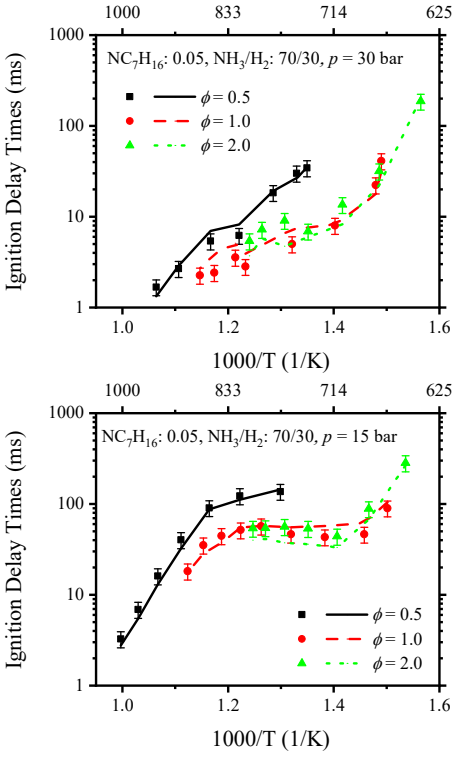

Figure 7. Measured (symbols) and calculated (lines) IDTs for NH_3/H_2/n-heptane mixtures with varying ϕ, at an NH_3/H_2 ratio of 70/30, and Pc of 30 bar and 15 bar.

Figure 7 shows the effect of equivalence ratio on IDTs when the NH_3/H_2 ratio is fixed at 70/30. As the equivalence ratio increases, the IDTs decrease. This behavior differs from the compression ignition of pure hydrogen-ammonia or pure ammonia mixtures without n-heptane, where the IDTs increase with the equivalence ratio [14]. Moreover, at ϕ = 0.5, the IDTs at both 15 bar and 30 bar show a significant increase compared to ϕ = 1 and ϕ = 2, indicating that lower equivalence ratios are more sensitive to IDTs in the current mixture, whereas higher equivalence ratios show lower sensitivity.

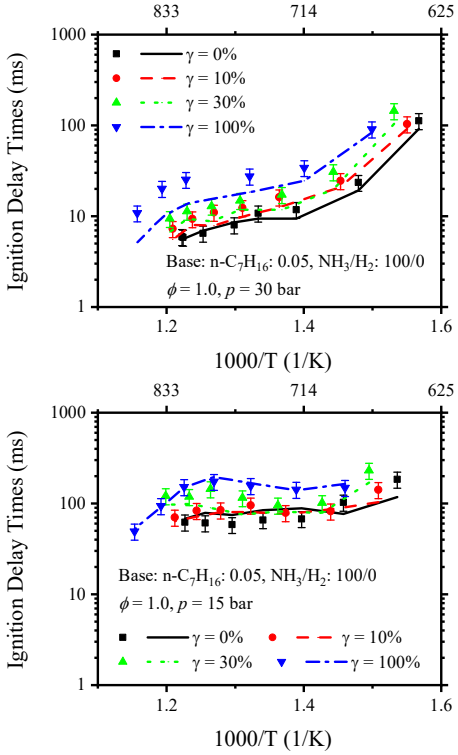

Figure 8. Measured (symbols) and calculated (lines) IDTs for NH_3/n-heptane mixtures with varying ammonia cracking ratios (γ) at ϕ = 1, with Pc of 30 bar and 15 bar. The γ is adjusted from a baseline Mixture1 where n-heptane accounts for 5% of the molar ratio, and the gaseous fuel initially consists entirely of ammonia.

The IDTs were measured under different ammonia cracking rates, with n-heptane constituting 5% of the total fuel molar ratio. In this study, the cracking rate γ for mixture 1 was defined as 0, representing pure ammonia, while a 100% cracking rate corresponds to ammonia fully decomposed into a 1:3 N_2/H_2 mixture. Overall, the IDTs at 15 bar were higher than those at 30 bar, and with increasing temperature, the IDT at the low-pressure condition decreased more gradually, showing lower sensitivity to temperature under the current test conditions.

Interestingly, unlike the typical trend where increasing H_2 content in a mixture reduces the IDTs, here, as the cracking rate increases, IDTs rise even though the H_2 content also increases. This counterintuitive behavior is attributed to the dilution effect caused by the introduction of N_2 from the cracking process. This is consistent with our

previous observation (Figure 6), which showed that altering NH_3/H_2 blending ratios does not significantly affect the IDTs for mixtures with n-heptane at high pressures and low temperatures. In these conditions, the reactivity of n-heptane dominates the overall ignition characteristics. As observed, with increasing hydrogen content, the promoting effect of hydrogen on IDTs is evident at temperatures above 690 K. However, for hydrogen produced through cracking, the dilution effect due to the N_2 outweighs the promoting effect of hydrogen, leading to longer IDTs at higher cracking rates.

The predictions from the current mechanism show excellent agreement with the RCM experimental data. In addition to the data measured here, we also validated the mechanism using high-pressure shock tube data from Dong et al. [48] for n-heptane/NH_3 mixtures. As shown in Figure 9, the current mechanism aligns well with their experimental data and even outperforms Dong et al.'s detailed mechanism in predicting their results.

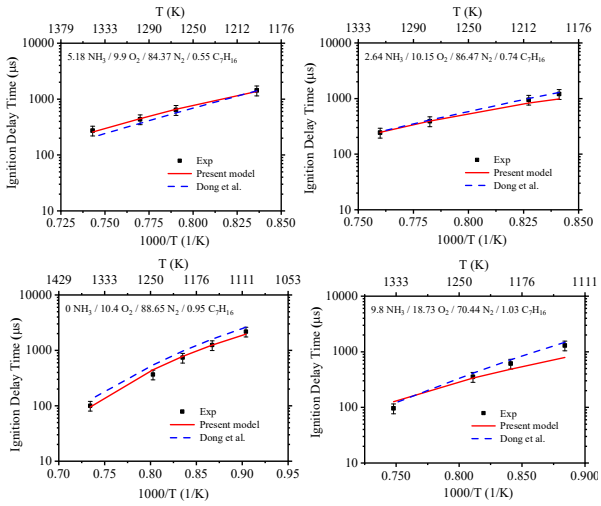

Figure 9. Comparison of Measured IDTs (symbols) of NH_3/n-heptane from Dong et al. [48], and simulated results (lines) from present model and Dong et al. [48] model.

4.1.2 VALIDATION OF LBVS

In addition to validating the reduced mechanism against our experimental data, it was extensively benchmarked against experimental literature data within the scope of the scenario-decoupled mechanism reduction method. This included comparisons of flame speeds for NH_3/H_2 and NH_3/n-heptane mixtures, which are critical for the current study. The significance of NH_3/H_2 flame speeds in the context of the partially cracked ammonia engine will be discussed in detail in the next section.

Figure 10 presents a comparison between experimental data from the literature and simulations of LBVs for NH_3/H_2 mixtures using the present reduced mechanism. The validation covers a wide range of conditions, including variations in hydrogen content, pressure, unburned gas temperature, and ammonia cracking ratio. Notably, the definition of γ in Mei et al. [15] aligns with that used in this study. As shown, LBVs increase with higher hydrogen content, elevated unburned gas temperatures, and reduced initial pressures.

The reduced mechanism retains all reactions from the NUIG2023 mechanism [45], and the optimization process deliberately avoided significant adjustments to reactions sensitive to flame speed. Therefore, the strong predictive performance of the reduced mechanism for NH_3/H_2 flame speeds can largely be attributed to the robust high-temperature NH_3 sub-mechanism in the NUIG2023 mechanism. Overall, the reduced mechanism demonstrates higher accuracy in predicting NH_3/H_2 flame speeds at low equivalence ratios. However, it slightly overestimates the flame speeds in the fuel-rich region. It is important to note that experimental measurements for the fuel-rich side in the literature exhibit considerable scatter [45].

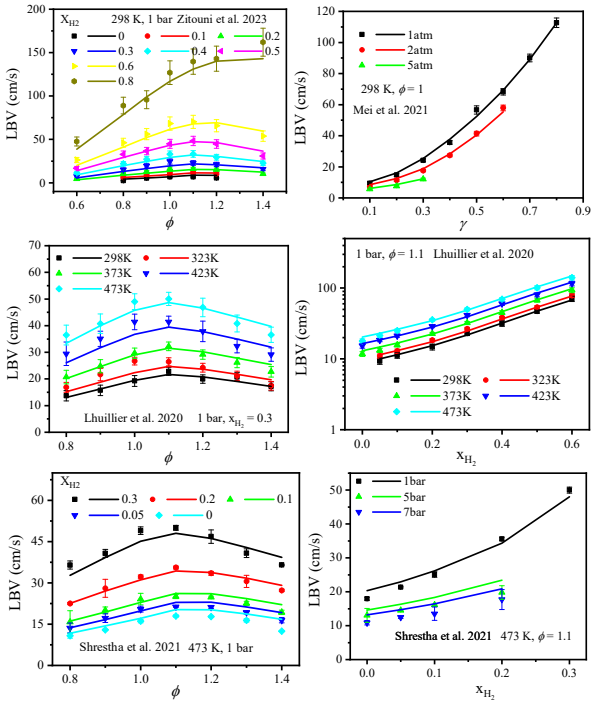

Figure 10. Comparison of experimental LBVs (symbols) from Zitouni et al. [49], Mei et al. [15], Lhuillier er al. [50] ,Shrestha et al. [51], and predictions (lines) from present model.

Figure 11 compares the experimental [52] and simulated LBVs of NH_3/n-heptane mixtures across

a ϕ range of 0.7 to 1.4. The predictions from the present reduced mechanism show good agreement with the experimental data, indicating satisfactory accuracy. The flame speed of the mixture is primarily governed by the presence of n-heptane. This type of validation corresponds to the local diffusion flame discussed earlier in the context of the mechanism development, representing the flame speed of vaporized n-heptane in an ammonia-dominated atmosphere. Due to the lack of experimental LBVs' measurements for NH_3/H_2/n-heptane mixture in the current literature, no comparisons for such cases are included.

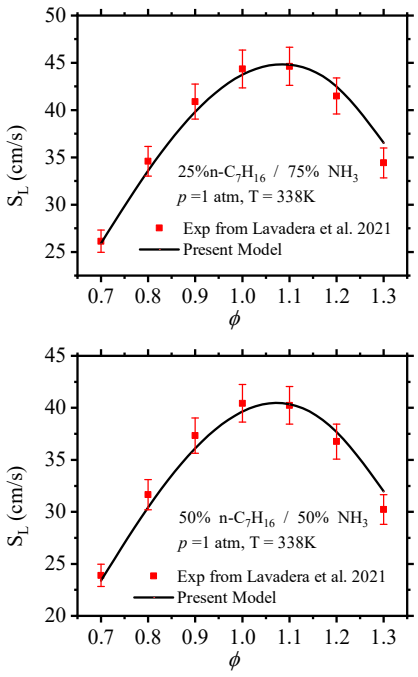

Figure 11. Comparison of experimental LBVs from Lavadera et al. [52] and calculations of present model as a function of equivalence ratio at 338 K and 1 atm.

Overall, the present reduced mechanism, developed through SDMRM, has demonstrated robust predictive accuracy for key combustion characteristics by extensive validation against experimental data. This reduced mechanism will be utilized for CFD simulations in the next section.

4.2 NUMERICAL SIMULATION RESULT

Unlike the molar ratio commonly used in fundamental combustion RCM experiments, fuel quantities in engines are often represented in terms of energy ratios. Table 3 presents the relationship between ammonia cracking ratios and the corresponding H_2/NH_3 energy ratios under the investigated CFD conditions.

Table 3. Corresponding H_2/NH_3 energy ratios for the ammonia cracking ratios investigated.

NH_3 cracking ratio(γ)	0%	4.42%	8.89%	18.00%	27.35%
H_2/NH_3 energy ratios	0/100	5/95	10/90	20/80	30/70

4.2.1 EXPLANATION OF NH_3/H_2 LBVS' IMPORTANCE

To highlight the importance of NH_3/H_2 LBV validation, CFD pre-simulation tests were conducted using the current engine model. Table 4 compares the temperature distribution contours in the main combustion chamber for cases with and without NH_3/H_2 mixtures, with the same amount of pilot diesel injected into the pre-chamber as the ignition fuel. All other operating conditions, including the cylinder pressure at top dead center (TDC), were kept identical by adjusting the intake air pressure.

Table 4. Temperature contours under identical operating conditions with and without gaseous fuels.

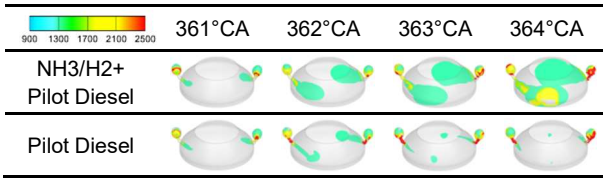

From Table 4 it can be observed that, in the case without NH_3/H_2 injection into the main combustion chamber, the flame emitted from the pre-chamber only affects a small region, with the majority of the space showing no temperature change. In contrast, when the main combustion chamber contains gaseous fuel, the temperature change affects a much larger area, with a trend of gradual expansion. As is generally understood for engines with pre-chamber structures, the combined effects of pre-chamber jet flame intensity and main chamber flame speed determine the engine's power output. The above comparison indicates that in the current engine configuration, the combustion of the premixed gaseous fuel predominantly governs the power output. Qualitatively, this suggests that the flame speed prediction of the NH_3/H_2 mixture plays a dominant role in the in-cylinder combustion process. It can also be inferred that, for engines without a pre-chamber structure and using direct-injection diesel ignition, the smaller the energy contribution from the ignition diesel, the more pronounced this effect becomes.

4.2.2 EFFECT OF EXCESS AIR COEFFICIENT ON COMBUSTION AND EMISSIONS

The current operating conditions fix the H_2/NH_3 energy ratio at 10/90, corresponding to an ammonia cracking rate of 8.89%. Figure 12 illustrates the impact of λ on engine performance and emissions. At high λ (e.g., 2.0), the lean premixed lean NH_3/H_2 mixture burns slowly, leading to lower cylinder temperatures and NOx emissions (0.745 g/kW·h). However, incomplete combustion results in 2.55% unburned ammonia, and engine power is significantly reduced. Reducing λ improves combustion efficiency by enhancing the burning of the premixed NH_3/H_2 mixture, leading to higher peak cylinder pressure, faster heat release, and increased engine power. As λ decreases, NOx emissions rise significantly due to higher cylinder temperatures. When λ is reduced from 1.8 to 1.7, NOx emissions increase by approximately 65%, surpassing the levels of the prototype diesel engine, while indicated power also decreases slightly. This highlights the trade-off with λ: lower values reduce unburned ammonia emissions but exacerbate NOx formation and slightly affect power output.

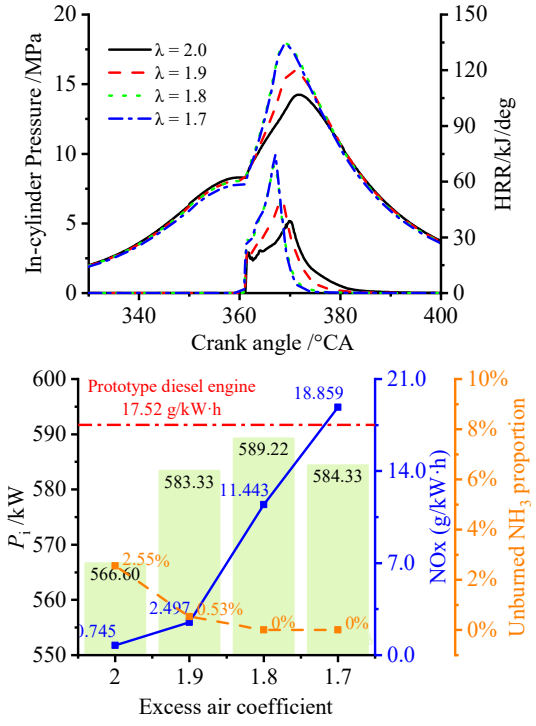

Figure 12. Combustion and emission performance under different λ at H_2/NH_3 energy ratio of 10/90.

Figure 13 shows the temperature contours under varying operating conditions. Following pilot diesel injection, a high-temperature zone forms in the pre-chamber and propagates into the main combustion chamber, igniting the premixed air and partially cracked ammonia products. This high-temperature region then expands gradually toward the cylinder walls. Lowering the λ, as shown in the contours, leads to earlier and faster flame penetration into the main chamber, indicating shorter IDTs. This advances jet flame formation and accelerates the flame propagation of the NH_3/H_2 mixture, enlarging the high-temperature region and raising overall cylinder temperatures. Consequently, NOx formation pathways are intensified, which explains why lower λ leads to higher NOx emissions.

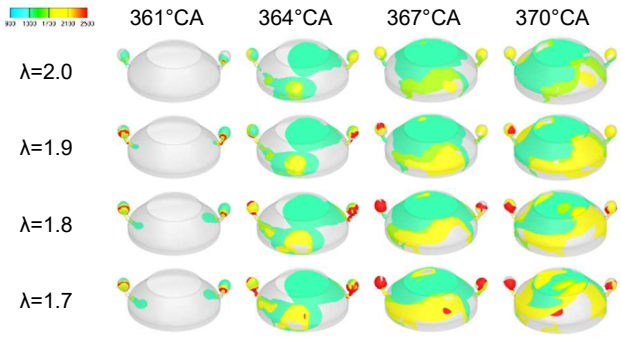

Figure 13. In-cylinder temperature contours at different crank angles under different λ at H_2/NH_3 energy ratio of 10/90.

4.2.3 EFFECT OF AMMONIA PARTIAL CRACKING RATIO ON COMBUSTION AND EMISSIONS

The current section discusses the variations in power performance and emission characteristics under different ammonia cracking ratios, represented as H_2/NH_3 energy ratios. Figure 14 compares the combustion and emission characteristics across varying H_2/NH_3 energy ratios, highlighting their significant influence on engine performance and emissions. From the cylinder pressure and heat release rate curves, even a small degree of ammonia cracking substantially improves the pressure rise rate, peak cylinder pressure, and peak heat release rate. Specifically, when the hydrogen energy ratio increases from 0% to 5%, the peak cylinder pressure rises by 16%, from 13.2 MPa (pure ammonia) to 15.29 MPa. This improvement is greater than the increments observed between higher hydrogen energy ratios, such as 10% to 20% and 20% to 30%, where peak pressure increases by approximately 6.4% and 9.5%, respectively. This trend in peak pressure is consistent with the variations in indicated power. The initial addition of a modest 5% hydrogen energy ratio from ammonia cracking leads to a significant improvement in indicated power. While the indicated power differences among the five cases are relatively small—except for the pure ammonia condition, where incomplete combustion results in lower power output—the influence of

ammonia cracking is clear. Although cracking introduces inert nitrogen gas, the enhanced combustion speed from the additional hydrogen outweighs the inhibitory effect of nitrogen. This improves combustion efficiency, reduces unburned ammonia, shortens the combustion duration, and significantly increases the peak heat release rate.

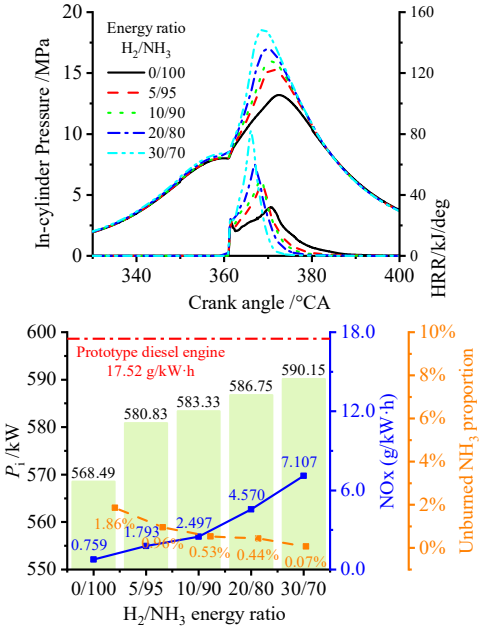

Figure 14. Combustion and emission performance under different H_2/NH_3 energy ratios at λ = 1.9.

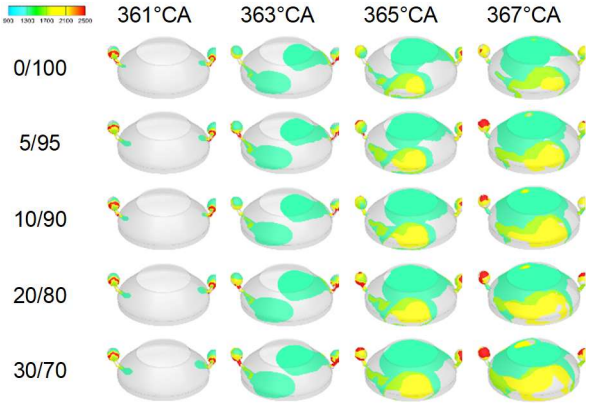

Figure 15. In-cylinder temperature contours under different H_2/NH_3 energy ratios at varying crank angles and λ = 1.9.

4.2.4 COMPREHENSIVE ANALYSIS OF OVERALL PERFORMANCE MAP

By expanding the research matrix to include varying γ and λ, Figure 16 provides a comprehensive comparison of emission performance, power output, and cylinder pressure behavior. These subplots visually reinforce the earlier conclusions while enabling a systematic analysis of the λ operating window under different γ. It should be noted that unburned ammonia emissions depend not only on the fraction of unburned ammonia but also on the total ammonia input. For example, at H_2/NH_3 ratios of 30/70 (λ = 2) and 5/95 (λ = 1.8), the unburned ammonia fractions are similar, but the 5/95 case results in 40% higher emissions in g/kW·h due to greater initial ammonia input. To address this, unburned ammonia emissions in g/kW·h are included in Figure 16 for a clearer comparison of environmental impact across conditions.

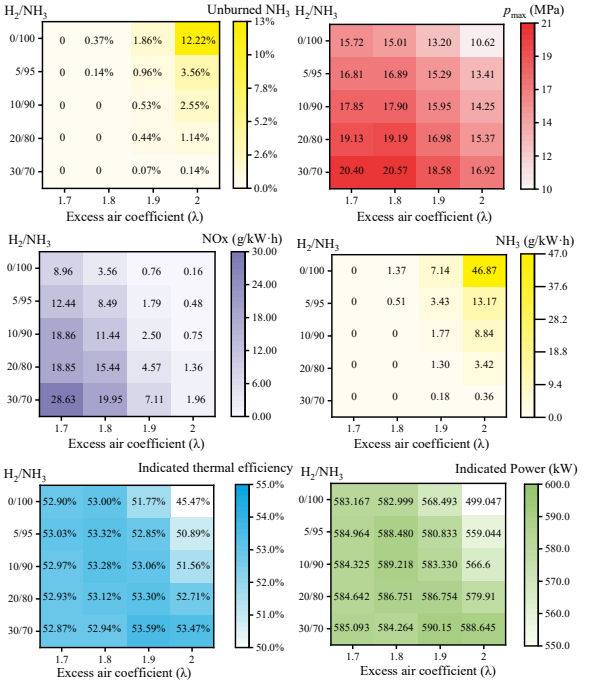

Figure 16. Comprehensive map analysis of power and emission performance under varied λ and H_2/NH_3 ratios (representing γ).

For conditions involving partially cracking ammonia, most performance indicators improve compared to pure ammonia operation. Unburned ammonia emissions, indicated power, and thermal efficiency benefit significantly from higher decomposition rates, especially at high λ. This highlights the limitations of ammonia's slow combustion in lean-burn conditions, which requires additional hydrogen to counteract the reduced flame speed and achieve combustion performance comparable to lower decomposition rates. Consequently, as shown in Figure 16, low decomposition rates and high λ result in suboptimal power and ammonia emission performance.

However, indicated power and thermal efficiency do not always exhibit a monotonic relationship with cracking ratios. For instance, at λ = 1.9, indicated power increases consistently with hydrogen content, whereas at λ = 1.7 and 1.8, it initially

increases and then decreases slightly, albeit with small overall variations.

Higher cracking ratios shift the engine toward hydrogen-dominant combustion. According to our prior studies [38], lean hydrogen mixtures are well-suited for large-bore two-stroke engines, where a sufficiently high λ not only reduces combustion temperatures to lower NOx emissions but also maintains acceptable combustion performance. This supports the conclusion that high decomposition rates and large λ values are beneficial for combustion in large two-stroke engines. However, a critical consideration for partially cracked ammonia engines is the efficiency and energy cost of online ammonia decomposition. Since decomposing ammonia into hydrogen and nitrogen requires additional energy, the practical feasibility of achieving very high cracking ratios is limited. Although higher cracking ratios bring combustion characteristics closer to those of hydrogen engines, the associated energy trade-offs necessitate careful optimization rather than unrestricted pursuit of maximum decomposition.

5 CONCLUSIONS

In this study, auto-ignition characteristics of a ternary fuel mixture consisting of NH_3/H_2 and n-heptane were experimentally investigated under high-pressure conditions using an RCM device. The self-ignition behavior of the mixture was analyzed across varying NH_3/H_2 ratios, pressures, and equivalence ratios, including scenarios with partial ammonia cracking. Based on the proposed SDMRM combined with the evolutionary algorithm, a reduced mechanism was developed and extensively validated, demonstrating strong predictive performance for the operation of PCAD engines. Subsequently, CFD simulations were conducted for a large-bore two-stroke engine with partial-cracking ammonia as the primary fuel and diesel pilot injection in the pre-chamber. The study explored the impact of different γ and λ on the engine's power and emission performance. The main conclusions are as follows:

1. The reduced mechanism constructed using the SDMRM combined with the evolutionary algorithm has been extensively validated against experimental combustion data, thus making it suitable for high-fidelity simulations of PCAD engines.

2. The IDTs of NH_3/H_2/n-heptane ternary fuels are primarily dominated by n-heptane. As the equivalence ratio increases, the IDTs decrease. While the NH_3/H_2 ratio has a relatively small effect on IDTs under high-pressure conditions, higher hydrogen content increases IDT sensitivity to temperature. In scenarios involving partially cracked ammonia, nitrogen introduced via ammonia decomposition acts as a diluent, prolonging IDTs despite the presence of hydrogen.

3. Lower λ advances the entry of flames into the main combustion chamber in PCAD engines, elevating combustion temperatures. This reduces unburned ammonia emissions but exacerbates NOx emissions. A moderate reduction in λ can improve combustion performance, slightly enhancing power output while keeping emissions manageable.

4. The hydrogen generated from ammonia decomposition significantly enhances combustion performance, outweighing the inhibitory dilution effect of extra nitrogen. Even minor partial cracking of ammonia can substantially increase combustion temperature, reduce unburned ammonia emissions, and improve indicated power. However, as hydrogen content continues to rise, the rate of performance improvement diminishes, and it simultaneously leads to progressively higher NOx emissions.

5. Increasing γ pushes the combustion process toward hydrogen-dominated behavior, favoring operating conditions with high λ for optimal performance. However, practical considerations, including the energy conversion efficiency and economic feasibility of on-site ammonia decomposition, must be carefully evaluated to achieve the most efficient and sustainable operation.

6 Definitions, Acronyms, Abbreviations

LBV: Laminar burning velocities

IDT: Ignition delay time

EA: Evolutionary algorithm

RCM: Rapid compression machine

SI: Spark-ignition

CI: Compression-ignition

CR: Compression ratio

EOC: End of compression

TDC: Top dead center

Pc: Compressed pressure

Tc: Compressed temperature

ϕ: Equivalence ratio

PCAD: Partial-cracking ammonia/diesel

HRR: Heat release rate

Q_{LHV}: Total energy introduced to the cylinder based on the lower heating value

SDMRM: Scenario-Decoupled Mechanism Reduction Method

NTC: Negative temperature coefficient

γ: Ammonia cracking ratios

λ: Excess air coefficient

7 ACKNOWLEDGMENTS

This work was supported by the Natural Science Foundations of China [grant number 52471315] and [grant number 52071061]; and the Research on combustion key technology of Otto-cycle ammonia engine combustion.

8 REFERENCES AND BIBLIOGRAPHY

[1] T. Ayvalı, S. C. Edman Tsang, and T. Van Vrijaldenhoven, The Position of Ammonia in Decarbonising Maritime Industry: An Overview and Perspectives: Part I : Technological advantages and the momentum towards ammonia-propelled shipping, *Johnson Matthey Technology Review,* vol. 65, no. 2, pp. 275-290, 2021.

[2] A. Valera-Medina *et al.*, Review on Ammonia as a Potential Fuel: From Synthesis to Economics, *Energy & Fuels,* vol. 35, no. 9, pp. 6964-7029, 2021/05/06 2021.

[3] H. Kobayashi, A. Hayakawa, K. D. Kunkuma A. Somarathne, and Ekenechukwu C. Okafor, Science and technology of ammonia combustion, *Proceedings of the Combustion Institute,* vol. 37, no. 1, pp. 109-133, 2019/01/01/ 2019.

[4] W. S. Chai, Y. Bao, P. Jin, G. Tang, and L. Zhou, A review on ammonia, ammonia-hydrogen and ammonia-methane fuels, *Renewable and Sustainable Energy Reviews,* vol. 147, p. 111254, 2021/09/01/ 2021.

[5] J. Tian *et al.*, Enhancing combustion efficiency and reducing nitrogen oxide emissions from ammonia combustion: A comprehensive review, *Process Safety and Environmental Protection,* vol. 183, pp. 514-543, 2024/03/01/ 2024.

[6] Y. Qi, W. Liu, S. Liu, W. Wang, Y. Peng, and Z. Wang, A review on ammonia-hydrogen fueled internal combustion engines, *eTransportation,* vol. 18, p. 100288, 2023/10/01/ 2023.

[7] Y. Feng *et al.*, Low-temperature auto-ignition characteristics of NH3/diesel binary fuel: Ignition delay time measurement and kinetic analysis, *Fuel,* vol. 281, p. 118761, 2020/12/01/ 2020.

[8] P. Dimitriou and R. Javaid, A review of ammonia as a compression ignition engine fuel, *International Journal of Hydrogen Energy,* vol. 45, no. 11, pp. 7098-7118, 2020.

[9] J. Tian *et al.*, Visualization study on ammonia/diesel dual direct injection combustion characteristics and interaction between sprays, *Energy Conversion and Management,* vol. 299, p. 117857, 2024/01/01/ 2024.

[10] X. Wang *et al.*, Exploring the GHG reduction potential of pilot diesel-ignited ammonia engines - Effects of diesel injection timing and ammonia energetic ratio, *Applied Energy,* vol. 357, p. 122437, 2024/03/01/ 2024.

[11] A. Yousefi, H. Guo, S. Dev, S. Lafrance, and B. Liko, A study on split diesel injection on thermal efficiency and emissions of an ammonia/diesel dual-fuel engine, *Fuel,* vol. 316, p. 123412, 2022/05/15/ 2022.

[12] M.-C. Chiong *et al.*, Advancements of combustion technologies in the ammonia-fuelled engines, *Energy Conversion and Management,* vol. 244, p. 114460, 2021/09/15/ 2021.

[13] H. Lesmana, M. Zhu, Z. Zhang, J. Gao, J. Wu, and D. Zhang, Experimental and kinetic modelling studies of flammability limits of partially dissociated NH3 and air mixtures, *Proceedings of the Combustion Institute,* vol. 38, no. 2, pp. 2023-2030, 2021/01/01/ 2021.

[14] L. Dai, S. Gersen, P. Glarborg, H. Levinsky, and A. Mokhov, Experimental and numerical analysis of the autoignition behavior of NH3 and NH3/H2 mixtures at high pressure, *Combustion and Flame,* vol. 215, pp. 134-144, 2020.

[15] B. Mei, J. Zhang, X. Shi, Z. Xi, and Y. Li, Enhancement of ammonia combustion with partial fuel cracking strategy: Laminar flame propagation and kinetic modeling investigation of NH3/H2/N2/air mixtures up to 10 atm, *Combustion and Flame,* vol. 231, p. 111472, 2021/09/01/ 2021.

[16] M. El-Adawy, M. A. Nemitallah, and A. Abdelhafez, Towards sustainable hydrogen and ammonia internal combustion engines: Challenges

and opportunities, *Fuel,* vol. 364, p. 131090, 2024/05/15/ 2024.

[17] M. Klawitter *et al.*, Ammonia as a fuel: Optical investigation of turbulent flame propagation of NH3/Air and NH3/H2/N2/Air flames at engine conditions, *Fuel,* vol. 375, p. 132616, 2024/11/01/ 2024.

[18] I. Lucentini, X. Garcia, X. Vendrell, and J. Llorca, Review of the Decomposition of Ammonia to Generate Hydrogen, *Industrial & Engineering Chemistry Research,* vol. 60, no. 51, pp. 18560-18611, 2021/12/29 2021.

[19] J. E. Lee, J. Lee, H. Jeong, Y.-K. Park, and B.-S. Kim, Catalytic ammonia decomposition to produce hydrogen: A mini-review, *Chemical Engineering Journal,* vol. 475, p. 146108, 2023/11/01/ 2023.

[20] A. Chapman *et al.*, A review of four case studies assessing the potential for hydrogen penetration of the future energy system, *International Journal of Hydrogen Energy,* vol. 44, no. 13, pp. 6371-6382, 2019/03/08/ 2019.

[21] D. Andriani and Y. Bicer, A Review of Hydrogen Production from Onboard Ammonia Decomposition: Maritime Applications of Concentrated Solar Energy and Boil-Off Gas Recovery, *Fuel,* vol. 352, p. 128900, 2023/11/15/ 2023.

[22] K. E. Lamb, M. D. Dolan, and D. F. Kennedy, Ammonia for hydrogen storage; A review of catalytic ammonia decomposition and hydrogen separation and purification, *International Journal of Hydrogen Energy,* vol. 44, no. 7, pp. 3580-3593, 2019/02/05/ 2019.

[23] S. Sun *et al.*, Ammonia as hydrogen carrier: Advances in ammonia decomposition catalysts for promising hydrogen production, *Renewable and Sustainable Energy Reviews,* vol. 169, p. 112918, 2022/11/01/ 2022.

[24] S. Frigo and R. Gentili, Analysis of the behaviour of a 4-stroke Si engine fuelled with ammonia and hydrogen, *International Journal of Hydrogen Energy,* vol. 38, no. 3, pp. 1607-1615, 2013/02/06/ 2013.

[25] C. Lhuillier, P. BREQUIGNY, F. Contino, and C. Rousselle, Performance and Emissions of an Ammonia-Fueled SI Engine with Hydrogen Enrichment, 2019. Available: https://doi.org/10.4271/2019-24-0137

[26] K. Ryu, G. E. Zacharakis-Jutz, and S.-C. Kong, Performance enhancement of ammonia-fueled engine by using dissociation catalyst for hydrogen generation, *International Journal of Hydrogen Energy,* vol. 39, no. 5, pp. 2390-2398, 2014/02/04/ 2014.

[27] M. Comotti and S. Frigo, Hydrogen generation system for ammonia–hydrogen fuelled internal combustion engines, *International Journal of Hydrogen Energy,* vol. 40, no. 33, pp. 10673-10686, 2015/09/07/ 2015.

[28] M. F. Ezzat and I. Dincer, Development and assessment of a new hybrid vehicle with ammonia and hydrogen, *Applied Energy,* vol. 219, pp. 226-239, 2018/06/01/ 2018.

[29] S. S. Gill, G. S. Chatha, A. Tsolakis, S. E. Golunski, and A. P. E. York, Assessing the effects of partially decarbonising a diesel engine by co-fuelling with dissociated ammonia, *International Journal of Hydrogen Energy,* vol. 37, no. 7, pp. 6074-6083, 2012/04/01/ 2012.

[30] B. Yan *et al.*, A critical review of NH3–H2 combustion mechanisms, *Renewable and Sustainable Energy Reviews,* vol. 196, p. 114363, 2024/05/01/ 2024.

[31] R. C. da Rocha, M. Costa, and X.-S. Bai, Chemical kinetic modelling of ammonia/hydrogen/air ignition, premixed flame propagation and NO emission, *Fuel,* vol. 246, pp. 24-33, 2019.

[32] K. P. Shrestha, L. Seidel, T. Zeuch, and F. Mauss, Detailed Kinetic Mechanism for the Oxidation of Ammonia Including the Formation and Reduction of Nitrogen Oxides, *Energy & Fuels,* vol. 32, no. 10, pp. 10202-10217, 2018.

[33] B. Mei *et al.*, Experimental and kinetic modeling investigation on the laminar flame propagation of ammonia under oxygen enrichment and elevated pressure conditions, *Combustion and Flame,* vol. 210, pp. 236-246, 2019.

[34] B. Mei, S. Ma, Y. Zhang, X. Zhang, W. Li, and Y. Li, Exploration on laminar flame propagation of ammonia and syngas mixtures up to 10 atm, *Combustion and Flame,* vol. 220, pp. 368-377, 2020/10/01/ 2020.

[35] X. Han, Z. Wang, Y. He, Y. Zhu, R. Lin, and A. A. Konnov, Uniqueness and similarity in flame propagation of pre-dissociated NH3 + air and NH3 + H2 + air mixtures: An experimental and modelling study, *Fuel,* vol. 327, p. 125159, 2022/11/01/ 2022.

[36] W. Qu *et al.*, Hydrogen/PRF skeletal mechanism study based on shock tube experiments and kinetic analysis, *Fuel,* vol. 333, p. 126342, 2023/02/01/ 2023.

[37] Z. Gong, M. Hu, Y. Fang, D. Zhang, and L. Feng, Mechanism study of natural gas pre-ignition induced by the auto-ignition of lubricating oil, *Fuel,* vol. 315, p. 123286, 2022/05/01/ 2022.

[38] W. Qu *et al.*, Hydrogen injection optimization of a low-speed two-stroke marine hydrogen/diesel engine, *Fuel,* vol. 366, p. 131352, 2024/06/15/ 2024.

[39] D. Lee and S. Hochgreb, Rapid Compression Machines: Heat Transfer and Suppression of Corner Vortex, *Combustion and Flame,* vol. 114, no. 3, pp. 531-545, 1998/08/01/ 1998.

[40] X. He, B. Shu, D. Nascimento, K. Moshammer, M. Costa, and R. X. Fernandes, Auto-ignition kinetics of ammonia and ammonia/hydrogen mixtures at intermediate temperatures and high pressures, *Combustion and Flame,* vol. 206, pp. 189-200, 2019.

[41] O. Mathieu and E. L. Petersen, Experimental and modeling study on the high-temperature oxidation of Ammonia and related NOx chemistry, *Combustion and Flame,* vol. 162, no. 3, pp. 554-570, 2015.

[42] X. Xu, Z. Wang, W. Qu, M. Song, Y. Fang, and L. Feng, Optimizations of energy fraction and injection strategy in the ammonia-diesel dual-fuel engine, *Journal of the Energy Institute,* vol. 112, p. 101455, 2024/02/01/ 2024.

[43] V. A. Alekseev and E. J. K. Nilsson, Reduced kinetics of NH3/n-heptane: Model analysis and a new small mechanism for engine applications, *Fuel,* vol. 367, p. 131464, 2024/07/01/ 2024.

[44] L. S. Thorsen *et al.*, High pressure oxidation of NH3/n-heptane mixtures, *Combustion and Flame,* vol. 254, 2023.

[45] Y. Zhu *et al.*, The combustion chemistry of ammonia and ammonia/hydrogen mixtures: A comprehensive chemical kinetic modeling study, *Combustion and Flame,* vol. 260, p. 113239, 2024/02/01/ 2024.

[46] S. Girhe *et al.*, Ammonia and ammonia/hydrogen combustion: Comprehensive quantitative assessment of kinetic models and examination of critical parameters, *Combustion and Flame,* vol. 267, p. 113560, 2024/09/01/ 2024.

[47] L. Elliott, D. B. Ingham, A. G. Kyne, N. S. Mera, M. Pourkashanian, and C. W. Wilson, Genetic algorithms for optimisation of chemical kinetics reaction mechanisms, *Progress in Energy and Combustion Science,* vol. 30, no. 3, pp. 297-328, 2004/01/01/ 2004.

[48] S. Dong *et al.*, An experimental and kinetic modeling study of ammonia/n-heptane blends, *Combustion and Flame,* vol. 246, 2022.

[49] S. Zitouni, P. Brequigny, and C. Mounaïm-Rousselle, Influence of hydrogen and methane addition in laminar ammonia premixed flame on burning velocity, Lewis number and Markstein length, *Combustion and Flame,* vol. 253, p. 112786, 2023/07/01/ 2023.

[50] C. Lhuillier, P. Brequigny, N. Lamoureux, F. Contino, and C. Mounaïm-Rousselle, Experimental investigation on laminar burning velocities of ammonia/hydrogen/air mixtures at elevated temperatures, *Fuel,* vol. 263, p. 116653, 2020/03/01/ 2020.

[51] K. P. Shrestha *et al.*, An experimental and modeling study of ammonia with enriched oxygen content and ammonia/hydrogen laminar flame speed at elevated pressure and temperature, *Proceedings of the Combustion Institute,* vol. 38, no. 2, pp. 2163-2174, 2021/01/01/ 2021.

[52] M. Lubrano Lavadera, X. Han, and A. A. Konnov, Comparative Effect of Ammonia Addition on the Laminar Burning Velocities of Methane, n-Heptane, and Iso-octane, *Energy & Fuels,* vol. 35, no. 9, pp. 7156-7168, 2020.